International Journal of Modern Physics C
Vol. 29, No. 6 (2018) 1850049 (16 pages)

DOI: 10.1142/S0129183118500493

World Scientific
www.worldscientific.com

Design of multiwing-multiscroll grid compound chaotic system and its circuit implementation

Wei Ai*, Kehui Sun† and Yuanli Fu‡
School of Physics and Electronics
Central South University
Changsha 410083, P. R. China
**aiwei123@csu.edu.cn*
†*kehui@csu.edu.cn*
‡*271166149@qq.com*

Received 24 November 2017
Accepted 10 May 2018
Published 14 June 2018

Based on the simplified Lorenz multiwing attractor and the generalized Jerk multiscroll attractor, the grid compound chaotic systems are designed via state variables exchanging, state variables scale transformation, coordinate transformation and switching control. By designing different switching controllers, four kinds of grid compound attractors are realized. Dynamical characteristics of these grid compound systems are analyzed by the means of phase diagram, Poincaré section, bifurcation diagram and the largest Lyapunov exponent (LLE). The digital circuit and analog circuit are designed, which verify the feasibility of the circuit implement of the compound chaotic system.

Keywords: Chaos; grid compound chaotic attractor; multiwing chaotic attractor; multiscroll chaotic attractor; circuit implementation.

PACS No.: 05.45.−a.

1. Introduction

In 1963, Lorenz found the first chaotic attractor in three-dimensional autonomous system when he studied the atmospheric convection.[1] Since then, the generalized Lorenz system has been extensively investigated.[2–5] To improve the performance of chaotic system, people began to study the strengthened chaotic system,[6] including multiwing chaotic system[7–9] and multiscroll chaotic system.[10,11] Actually, a variety of design methods were proposed to generate multiwing chaotic attractor, such as heteroclinic orbits method,[12] fractal method,[13–15] and piecewise linear control method.[16,17] Meanwhile, many nonlinear functions were also employed to generate multiscroll attractor, such as step wave and saturated sequence,[18–20] hyperbolic tangent function series.[21] Compared with single type chaotic system, compound

† Corresponding author.

chaotic system has richer dynamic characteristic, so designing new control methods for constructing complex chaotic attractors has become a hot topic in recent years. For example, Ref. 22 constructed compound chaotic attractors among the Lorenz system family by designing the switching controller, and its analog circuit was implemented with traditional operational amplifiers only for the same type of chaotic attractors. Reference 23 constructed compound attractors with multiwing and multiscroll chaotic attractors, and it was verified by circuit simulation. However, these systems were constructed with simple one-dimensional compound chaotic attractors, and the characteristic analysis of the compound system was not involved. An interesting question is whether one can design a multiwing-multiscroll grid compound chaotic system, which may have a more complex topological structure.

Circuit implementation is meaningful for the chaos application.[24–26] Analog circuit can generate real chaotic signal, and digital circuit can generate chaotic signal more conveniently and controllably. Nowadays, current conveyor has been widely applied to realize simple chaotic circuits.[27–29] Meanwhile, DSP implementation of chaotic systems is repeatable, stable and reliable.[30] So we will take the current conveyor circuit and DSP platform as experimental verification for the designing of grid compound chaotic systems.

In this paper, taking the simplified Lorenz multiwing chaotic attractor[31] and the generalized Jerk multiscroll chaotic attractor as the basic systems,[32] we designed four kinds of compound chaotic systems. The rest of this paper is organized as follows. The compound chaotic systems are designed in Sec. 2. The dynamics of the compound chaotic attractors are analyzed in Sec. 3. The circuit implementation is presented in Sec. 4. Finally, we summarize the conclusions.

2. Design of the Grid Compound Chaotic System

2.1. *Design principle*

There are 4 main steps to obtain compound chaotic attractors.[22] Considering N three-dimensional chaotic systems, the design steps are presented as follows:

Step 1. Exchange state variables of the systems to ensure that all these chaotic attractors are located in different regions in the same phase space.
Step 2. Transform the scale of the state variables of all the N chaotic systems to ensure that each generated attractor has appropriate and comparable sizes in the phase space.
Step 3. Transform the coordinates in an appropriate direction for the systems so that each pair of adjacent chaotic attractors has a common connected domain.
Step 4. Generate a compound chaotic attractor via switching control based on the N chaotic systems.

The multiscroll-multiwing chaotic system is compounded by switching control. Through the combination of different transformations with switch controllers, we designed four kinds of the grid compound chaotic systems as shown in Fig. 1.

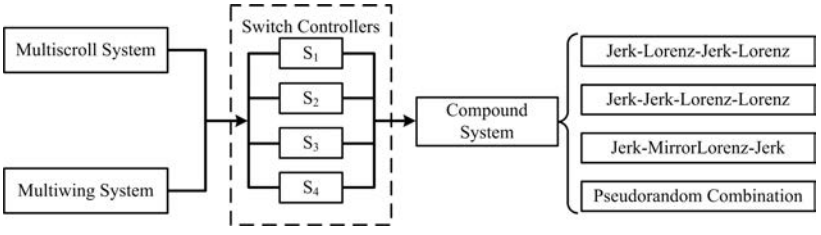

Fig. 1. Block diagram of the design principle.

2.2. *Models of the basic compound chaotic system*

By replacing a nonlinear cross-product in the simplified Lorenz system[31] with a multisegment quadratic function $F(x_1)$, the simplified Lorenz multiwing chaotic system is obtained as

$$\begin{cases} \dot{x}_1 = 10(y_1 - x_1), \\ \dot{y}_1 = (24 - 4c)x_1 - px_1z_1 + cy_1, \\ \dot{z}_1 = F(x_1) - (8/3)z_1, \\ F(x_1) = F_0{x_1}^2 - \sum_{i=1}^{N} F_i(1 + 0.5(x_1 - E_i) - 0.5(x_1 + E_i)), \end{cases} \tag{1}$$

where c is the system parameter, and p is the constant, which can facilitate the design and implementation of the corresponding circuits. N, F_0, F_i and E_i are the adjustable parameters.

The generalized Jerk multiscroll chaotic system is written as[32]

$$\begin{cases} \dot{x}_2 = y_2, \\ \dot{y}_2 = z_2, \\ \dot{z}_2 = -x_2 - y_2 - \beta z_2 + G(x_2), \\ G(x_2) = A\,\mathrm{sgn}(x_2) + A\sum_{n=1}^{N} \mathrm{sgn}(x_2 - 2nA) + A\sum_{n=1}^{N} \mathrm{sgn}(x_2 + 2nA), \end{cases} \tag{2}$$

where β is the system parameter, and A is the constant. $G(x_2)$ is the nonlinear term, which can control the number of scrolls. The switch controllers S_1, S_2 are designed as

$$\begin{cases} S_1 = 0.5(1 + \mathrm{sgn}(z - z_0)), \\ S_2 = 0.5(1 - \mathrm{sgn}(z - z_0)), \end{cases} \tag{3}$$

where z_0 is the switching control point, and it should be located in common connected domain of the two attractors. According to the compound principle, the Eqs. (1) and (2) are in different phase planes, then we exchange the state variable y_2 and z_2 of Eq. (2). In order to ensure that every generated attractor has appropriate and comparable size in the phase space, we expand 10 times of the state variable x_1 in Eq. (1), then the one-dimensional multiwing-multiscroll compound chaotic attractor

system is designed as

$$\begin{cases} \dot{x} = (z-l)S_1 + 100(y-0.1x)S_2, \\ \dot{y} = (-x-(z-l)-\beta y + G(x))S_1 + (0.1(24-4c)x - 0.1pxz + cy)S_2, \\ \dot{z} = yS_1 + (F(0.1x) - (8/3)z)S_2, \end{cases} \tag{4}$$

where $G(x)$ and $F(x)$ are defined by Eqs. (1) and (2), respectively. When $c = 1$, $p = 20, F_0 = 400, F_1 = -20.5, E_1 = 0.2, \beta = 0.75, A = 1, N = 1, M = 1, l = 3.5, z_0 = 2.4$, we obtained the compound chaotic attractor and time domain waveform as shown in Figs. 2(a) and 2(b), respectively, and its Poincaré section is shown in Fig. 2(c), which is calculated with $y = 0$ as a cross-section. It shows the four-wing and four-scroll attractor is generated and the compound system is chaotic.

2.3. *Design of the Jerk–Lorenz–Jerk–Lorenz compound chaotic system*

According to Sec. 2.1, the grid compound Jerk–Lorenz–Jerk–Lorenz system is designed by

$$\begin{cases} \dot{x} = (z-l_2)S_1 + 100(y-0.1x)S_2 + (z-l_1-f(z))S_3 + 100(y-0.1x)S_4, \\ \dot{y} = (-x-(z-l_2)-\beta y + G(x))S_1 + (0.1(24-4c)x - 0.1pxz + cy)S_2, \\ \quad + (-x-z+l_1+f(z)-\beta y + G(x))S_3 + (0.1(24-4c)x \\ \quad - 0.1px(z-f(z)) + cy)S_4, \\ \dot{z} = yS_1 + (F(0.1x) - (8/3)z)S_2 + yS_3 + (F(0.1x) - (8/3)(z-f(z)))S_4, \end{cases} \tag{5}$$

where $l_1 = 3.7, l_2 = 3.1, p = 20, c = 1, \beta = 0.75$, and $S_1, S_2, S_3, S_4, f(z), F(x)$ are designed as

$$\begin{cases} S_1 = 0.5(1 - \mathrm{sgn}(z - z_{01})), \\ S_2 = 0.5(\mathrm{sgn}(z - z_{01}) - \mathrm{sgn}(z - z_{02})), \\ S_3 = 0.5(\mathrm{sgn}(z - z_{02}) - \mathrm{sgn}(z - z_{03})), \\ S_4 = 0.5(1 + \mathrm{sgn}(z - z_{03})), \\ f(z) = A(1 + \mathrm{sgn}(z - z_{02})), \\ F(x) = F_0 x^2 - \sum_{i=1}^{N} F_i(1 + 0.5(x - E_i) - 0.5(x + E_i)), \end{cases} \tag{6}$$

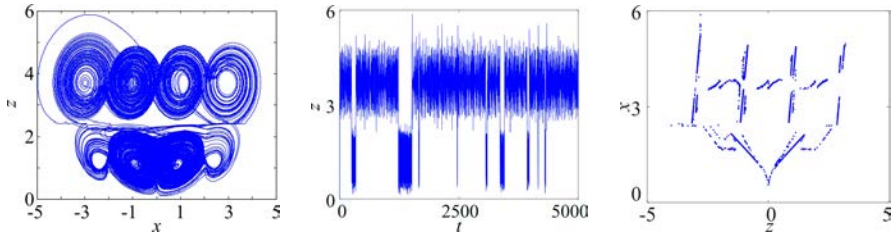

(a) (b) (c)

Fig. 2. Numerical simulations of the compound chaotic attractor: (a) Phase diagram on $x - z$ plane, (b) Time domain waveform of variable z, (c) Poincaré section ($y = 0$).

where $z_{01}=2.3, z_{02}=4.4, z_{03}=6.7, A=2.05, N=1, F_0=400, F_1=-20.5, E_1=0.2$. S_1, S_2, S_3, S_4 are the switching controllers, and $f(z)$ is the displacement function of the Lorenz system. According to Eqs. (5) and (6), we set the initial value $(x, y, z) = (0.1, 0.1, 0.1)$, and the attractor and its Poincaré section with $y = 0$ are shown in Figs. 3(a) and 3(c), respectively. The time domain waveform of this system is also plotted as shown in Fig. 3(b). Obviously, the system is chaotic, and the largest Lyapunov exponent (LLE) of the compound system is 8.6247, which indicates the chaotic system is very complicated.

2.4. *Design of the Jerk–Jerk–Lorenz–Lorenz compound chaotic system*

According to the design principle, the grid compound Jerk–Jerk–Lorenz–Lorenz chaotic system is obtained as

$$\begin{cases} \dot{x} = 100(y - 0.1x)S_1 + (z - f_1(z))S_2, \\ \dot{y} = (0.1(24 - 4c)x - 0.1px(z - f_2(z) - l_1) + cy)S_1 \\ \qquad + (-x - (z - f_1(z)) - \beta y + G(x))S_2, \\ \dot{z} = (F(0.1x) - (8/3)(z - f_2(z) - l_1))S_1 + yS_2, \end{cases} \tag{7}$$

where $S_1, S_2, g(x), f_1(z), f_2(z), F(x)$ are designed as

$$\begin{cases} S_1 = 0.5(1 + \mathrm{sgn}(z - z_0)), \\ S_2 = 0.5(1 - \mathrm{sgn}(z - z_0)), \\ g(x) = \mathrm{sgn}(x) + \mathrm{sgn}(x - 2) + \mathrm{sgn}(x + 2), \\ f_1(z) = 0.5A_1(1 + \mathrm{sgn}(z - l_1)), \\ f_2(z) = A_2(1 + \mathrm{sgn}(z - l_2 - l_3)), \\ F(x) = F_0x^2 - \sum_{i=1}^{N} F_i(1 + 0.5(x - E_i) - 0.5(x + E_i)), \end{cases} \tag{8}$$

here, $c = 1, \beta = 0.75, p = 20, l_1 = 1.1, l_2 = 2.4, l_3 = 3.5, A_1 = 2.1, A_2 = 1.1, z_0 = 3.5$, $N = 1, F_0 = 400, F_1 = -20.5, E_1 = 0.2$. z_0 is the boundary between the Lorenz system and the Jerk system, and l_1 is the displacement distance of the Lorenz system. $f_1(z)$ is the displacement function of Jerk system, and $f_2(z)$ is the Lorenz translation

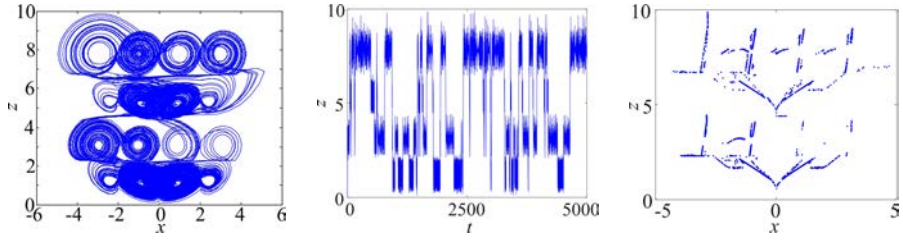

(a) (b) (c)

Fig. 3. Numerical simulations of the Jerk–Lorenz–Jerk–Lorenz compound chaotic attractor: (a) Phase diagram on x–z plane, (b) Time domain waveform of variable z, (c) Poincaré section ($y = 0$).

function. S_1 and S_2 are the switching function. The compound attractor, time domain waveform and Poincaré section at $y = 0$ are shown in Fig. 4. It indicates this grid compound system is chaotic.

2.5. *Design of the Jerk–MirrorLorenz–Jerk compound chaotic system*

Replacing the variable z with a mirror transformation function $\text{sgn}(z - z_0) \times (z - z_0) + z_0 - g(z)$ in Eq. (1), and the mirror Lorenz system becomes to

$$\begin{cases} \dot{x} = 100(y - 0.1x), \\ \dot{y} = 0.1(24 - 4c)x - 0.1px(\text{sgn}(z - z_0)(z - z_0) + z_0 - g(z)) + cy, \\ \dot{z} = \text{sgn}(z - z_0)F(x) - (8/3)(z - z_0) - 8/3\,\text{sgn}(z - z_0)(z_0 - g(z)), \end{cases} \tag{9}$$

and then the Jerk–MirrorLorenz–Jerk compound system is obtained as

$$\begin{cases} \dot{x} = (z - l_1)S_1 + 100(y - 0.1x)S_2 + (z - l_2)S_3, \\ \dot{y} = (-x - (z - l_1) - \beta y + g(x))S_1 + (0.1(24 - 4c)x - 0.1px(\text{sgn}(z - z_0)(z - z_0) \\ \quad + z_0 - g(z)) + cy)S_2 + (-x - (z - l_2) - \beta y + g(x))S_3, \\ \dot{z} = yS_1 + (\text{sgn}(z - z_0)F(0.1x) - (8/3)(z - z_0) \\ \quad - 8/3\,\text{sgn}(z - z_0)(z_0 - g(z)))S_2 + yS_3, \end{cases} \tag{10}$$

where $S_1, S_2, S_3, g(x), g(z)$, and $F(x)$ are designed by

$$\begin{cases} S_1 = 0.5(\text{sgn}(z - j_1) - \text{sgn}(z - j_2)), \\ S_2 = 0.5(\text{sgn}(z - l_3) - \text{sgn}(z - l_4)), \\ S_3 = 0.5(\text{sgn}(z - j_3) - \text{sgn}(z - j_4)), \\ g(x) = \text{sgn}(x) + \text{sgn}(x - 2) + \text{sgn}(x + 2), \\ g(z) = \sum_{i=1}^{M_2} (\pm A(1 \pm \text{sgn}(\text{sgn}(z - z_0)(z - z_0) - (z_i - z_0)))), \\ F(x) = F_0 x^2 - \sum_{i=1}^{N} F_i(1 + 0.5(x - E_i) - 0.5(x + E_i)), \end{cases} \tag{11}$$

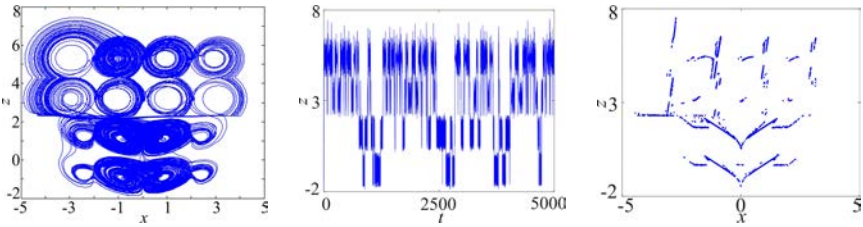

(a) (b) (c)

Fig. 4. Numerical simulations for Jerk–Jerk–Lorenz–Lorenz grid compound chaotic attractor: (a) Phase diagram on x–z plane, (b) Time domain waveform of variable z, (c) Poincaré section ($y = 0$).

where the values of A, z_0 and z_i are obtained by trial and error method, and M_2 is nonnegative integer. When $c = 1, p = 20, F_0 = 400, F_1 = -20.5, E_1 = 0.2, \beta = 0.75, A = 1.1, N = 1, M_2 = 1, z_0 = 0.2, z_1 = 2.8, j_1 = 2.45, j_2 = j_1 + 5, j_3 = l_3 - 5, j_4 = l_3, l_1 = 3.3, l_2 = -3.05, l_3 = -1.95, l_4 = 2.45$, the grid compound attractor, time domain waveform and Poincaré section at $y = 0$ are shown in Fig. 5. It is clear that the grid compound system is chaotic.

2.6. *Design of the pseudorandom compound chaotic system*

To improve the performance of the compound system further, we designed a compound chaotic system by employing pseudorandom switch method. It is defined by

$$\begin{cases} \dot{x} = 100(y - 0.1x)S_1 + (z - f_3(z) - j_2)S_2 + (z - f_1(z))S_3, \\ \dot{y} = (0.1(24 - 4c)x - 0.1px(z - f_2(z) - l_3) + cy)S_1 \\ \qquad + (-x - (z - f_3(z)) - j_2 - \beta y + g(x))S_2 + (-x - (z - f_1(z)) - \beta y + g(x))S_3, \\ \dot{z} = (F(0.1x) - (8/3)(z - f_2(z) - l_3))S_1 + yS_2 + yS_3, \end{cases} \tag{12}$$

where the switching controllers S_1, S_2 and S_3 are designed by

$$\begin{cases} S_1 = 0.5(1 + \mathrm{sgn}(z - z_0))W_1(z), \\ S_2 = 0.5(1 - \mathrm{sgn}(z - z_0)), \\ S_3 = 0.5(1 + \mathrm{sgn}(z - z_0))W_2(z), \end{cases} \tag{13}$$

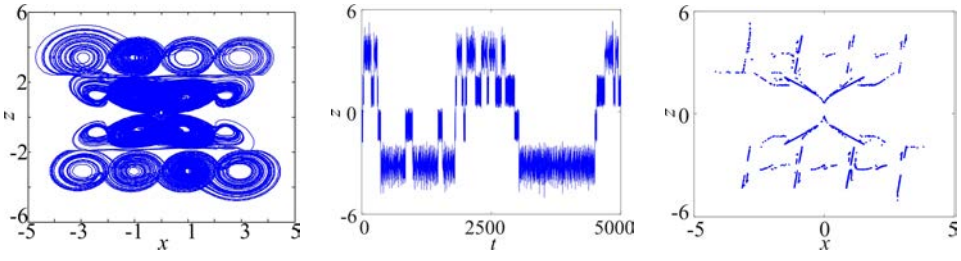

(a) (b) (c)

Fig. 5. Numerical simulations of the Jerk–MirrorLorenz–Lorenz compound chaotic attractor: (a) Phase diagram on x–z plane, (b) Time domain waveform of variable z, (c) Poincaré section ($y = 0$).

and the functions are designed as

$$\begin{cases} W_1(z) = 0.5(1 + \mathrm{sgn}(U_1(z) - W_1(z)))U_1(z) + 0.5(1 - \mathrm{sgn}(U_1(z) - W_1(z)))W_1(z), \\ W_2(z) = 0.5(1 + \mathrm{sgn}(U_2(z) - W_2(z)))U_2(z) + 0.5(1 - \mathrm{sgn}(U_2(z) - W_2(z)))W_2(z), \\ U_1(z) = 0.5(1 + \mathrm{sgn}(R - 50)), \\ U_2(z) = 0.5(1 - \mathrm{sgn}(R - 50)), \\ f_1(z) = 0.5A_1(1 + \mathrm{sgn}(z - l_1)), \\ f_2(z) = A_2(1 + \mathrm{sgn}(z - l_2 - l_3)), \\ f_3(z) = A_2(1 + \mathrm{sgn}(z - j_1 - j_2)), \\ F(x) = F_0x^2 - \sum_{i=1}^{N} F_i(1 + 0.5(x - E_i) - 0.5(x + E_i)), \end{cases} \tag{14}$$

where $f_1(z), f_2(z), f_3(z)$ are the parallel transformation functions. A_1, A_2 are constants, j_1, j_2, l_1, l_2, l_3 are the space displacements, and they are obtained by trial-and-error method. Obviously, this compound system is uncertain before the initial values of chaotic system are selected, so it will be more appropriate than other chaotic systems when it is applied to secure communication. For simplicity, we set the switching controller S_2 be always valid, and it determines that the half of this system is Jerk system with 2×4 scrolls. There is only one effective controller between S_1 and S_3, and they eventually determine the type of system to be generated. The flow diagram is shown in Fig. 6.

Setting $j_1 = 1.1, j_2 = 6.1, c = 1, \beta = 0.75, p = 20, z_0 = 3.5, l_1 = 1.1, l_2 = 2.4, l_3 = 3.5, A_1 = 2.1, A_2 = 1.1, N = 1, F_0 = 400, F_1 = -20.5, E_1 = 0.2$, and changing initial values, the two kinds of compound chaotic systems appear randomly as shown in Figs. 7(a) and 7(d), respectively. Here, we get the sum of decimal part of initial three coordinates, and then let it fall into a specific interval by numerical processing, and the result is R. When R falls into the half of this interval, Fig. 7(a) appears. Otherwise, Fig. 7(d) shows up. When R is obtained, one of the groups in $U_1(z)$, $W_1(z), S_1$ and $U_2(z), W_2(z), S_3$ are selected. S_1, S_2, S_3 are switch controllers. $W_1(z)$ and $W_2(z)$ determine which switch controller is valid between S_1 and S_3.

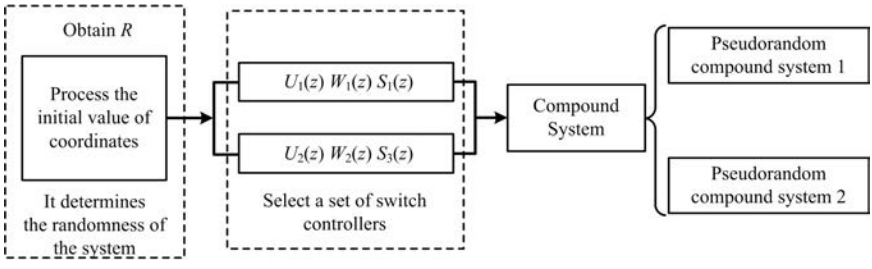

Fig. 6. Flow diagram of pseudorandom switch method.

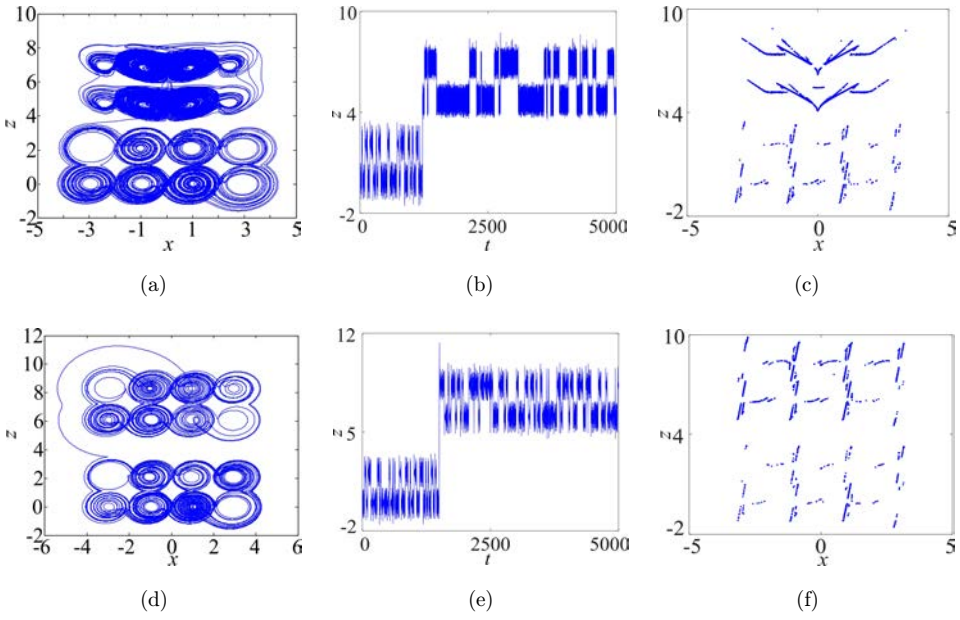

Fig. 7. Numerical simulations of the pseudorandom compound system: (a) Phase diagram on x–z plane, (b) Time domain waveform of variable z, (c) Poincaré section ($y = 0$), (d) Phase diagram on x–z plane, (e) Time domain waveform of variable z, (f) Poincaré section ($y = 0$).

Apparently, it is more difficult for people to predict the orbit of the chaotic attractor. So, this approach can be used to obtain more complicated attractors. It is worth mentioning that the randomness of the compound system can not only be determined by the initial value, but also by other factors.

3. Dynamics of the Grid Compound Chaotic System

3.1. *Lyapunov exponents*

The Lyapunov exponents of different grid compound chaotic systems are shown in Fig. 8. It can be seen that the Lyapunov exponents of Jerk–Lorenz are similar to that of the 1×4-wing Lorenz system when $c > 2$. The Lyapunov exponents of Jerk–Jerk–Lorenz–Lorenz are similar to that of the 1×4-wing Lorenz system when $c > 0.5$. The Lyapunov exponents of Jerk–Lorenz–Jerk–Lorenz are similar to that of the 1×4-wing Lorenz system when $c > 0$. The Lyapunov exponents of Jerk–MirrorLorenz–Jerk are similar to that of the 1×4-wing Lorenz system when $c \in (2, 6)$. It shows that the compound system still contains the dynamic properties of subsystems.

3.2. *The LLE analysis*

The LLE[33] of the grid compound systems are listed in Table 1. The Jerk–Lorenz–Jerk–Lorenz system has the largest LLE, which means it has more complex

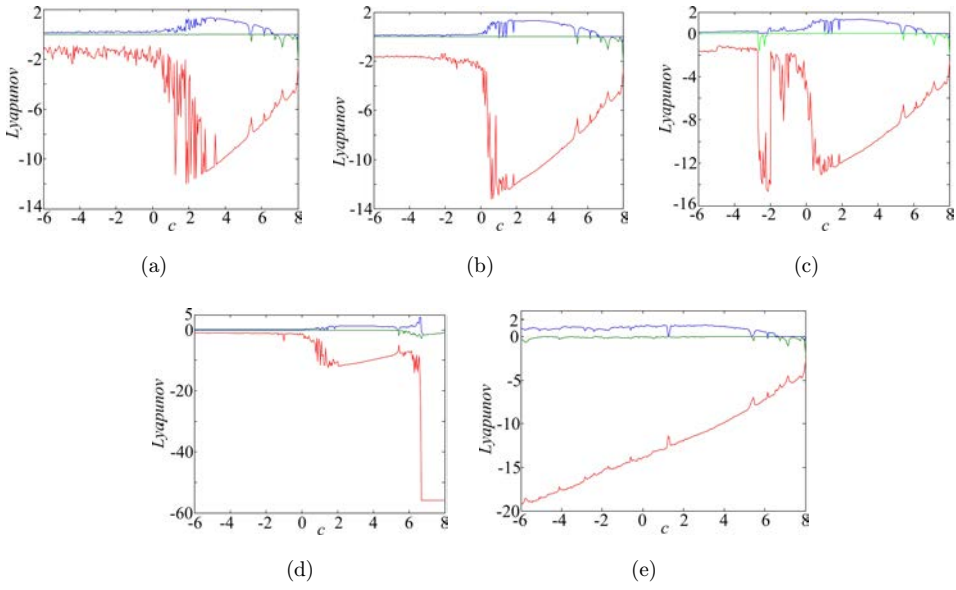

Fig. 8. The Lyapunov exponents of different compound chaotic systems: (a) Jerk–Lorenz, (b) Jerk–Jerk–Lorenz–Lorenz, (c) Jerk–Lorenz–Jerk–Lorenz, (d) Jerk–MirrorLorenz–Jerk, (e) 1×4-wing Lorenz.

Table 1. The LLE of different compound attractors.

Chaotic systems	LLE ($c = 1, \beta = 0.75$)
Multiwing chaotic attractor (1×4 Lorenz)	1.7180
Multiscroll chaotic attractor (1×4 Jerk)	0.0602
Parallel transform multiwing chaotic attractor (4×4 Lorenz)	1.8781
Parallel transform multiscroll chaotic attractor (4×4 multiscroll)	0.0698
Multiwing-multiscroll compound (1×4 Jerk-1×4 Lorenz)	0.5562
Multiwing-multiscroll grid compound (Jerk–Jerk–Lorenz–Lorenz)	6.8354
Multiwing-multiscroll mirror compound (Jerk–MirrorLorenz–Jerk)	1.8312
Multiwing-multiscroll cross grid compound (Jerk–Lorenz–Jerk–Lorenz)	8.6247

dynamical behaviors. The LLE of Jerk–Lorenz system stays between that of Jerk system and Lorenz system, while the LLE of Lorenz–Lorenz–Jerk–Jerk does not increased apparently. It can be seen that the complexity of the grid compound attractor is improved by suitable combination control.

3.3. *Chaotic graph of the Jerk–Lorenz–Jerk–Lorenz chaotic system*

As the Jerk–Lorenz–Jerk–Lorenz and Jerk–Jerk–Lorenz–Lorenz have the larger LLE, we focus on the dynamical properties of the two systems. Chaos diagram is a comprehensive way to reflect dynamics of a chaotic system in the parameter space. As shown in Fig. 9, the darker the color is, the larger the LLE is, and it indicates that the chaotic system is more complex. When it is applied to secure communication,

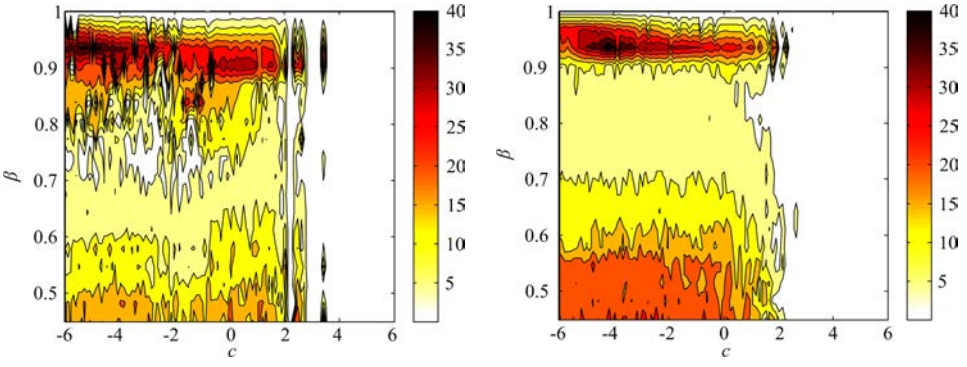

Fig. 9. Chaotic diagrams for the different compound chaotic systems: (a) The Jerk–Lorenz–Jerk–Lorenz system, (b) The Jerk–Jerk–Lorenz–Lorenz system.

the parameters of system should be selected in darker areas. While changing compound systems parameters c and β, respectively, the maximum value of LLE reachs 40. One can choose the most suitable parameters from this diagram in applications. For Fig. 9(a), we found that when the parameter $c \in (-6, 3)$,

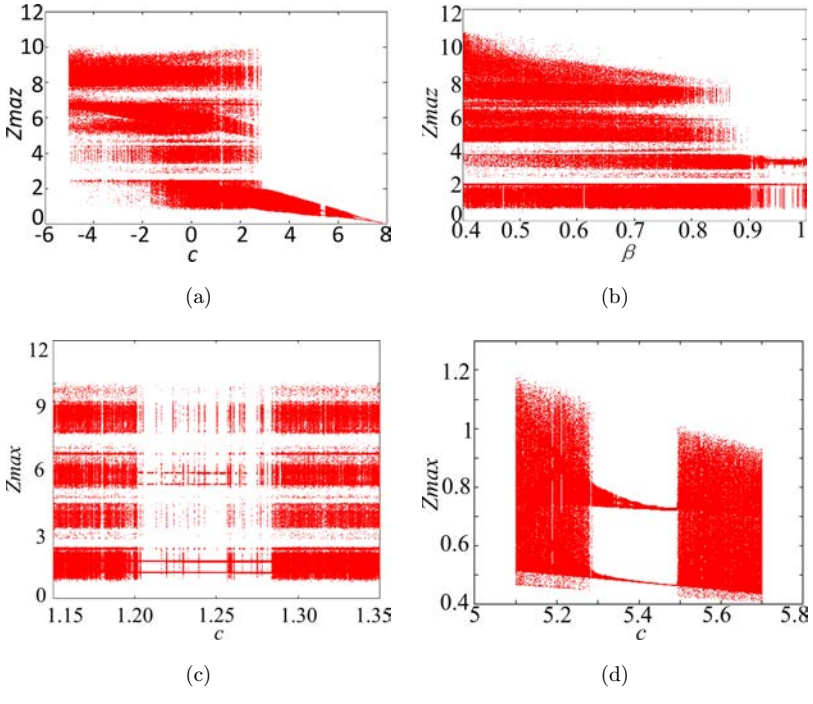

Fig. 10. Bifurcation diagram of the Jerk–Lorenz–Jerk–Lorenz chaotic system: (a) $\beta = 0.75, c \in [-5, 8]$, (b) $c = 1, \beta \in [0.4, 1]$, (c) $\beta = 0.75, c \in [1.1, 1.4]$, (d) $\beta = 0.75, c \in [5.1, 5.7]$.

$\beta \in (0.9, 0.98)$, the system has larger LLE in most area. When $\beta \in (0.6, 0.85)$, the LLE is relatively smaller. For Fig. 9(b), when the parameter $c \in (-6, 2)$, $\beta \in (0.9, 0.98)$, the system has larger LLE in most area, and β should be avoided the values at the range (0.7, 0.9).

3.4. *Bifurcation of the Jerk–Lorenz–Jerk–Lorenz chaotic system*

The bifurcation diagrams of the compound system about c and β are shown in Figs. 10(a) and 10(b), respectively. It is found that the system is chaotic over most of the rang $c \in [-6, 7]$. There are two apparent periodic windows at $c \in (1.21, 1.27) \cup (5.28, 5.5)$ as shown in Fig. 10(a). It is consistent with the Lyapunov exponent diagram as shown in Fig. 8(c). To display it clearly, the magnified diagrams are shown in Figs. 10(c) and 10(d). There exist a pitchfork bifurcation, flip bifurcation and interior crisis in Fig. 10(d). It is observed from Fig. 10(b) that the grid compound system is chaotic when $c = 1$ and $\beta \in [0.4, 1]$.

4. Circuit Design and Implementation

4.1. *Analog circuit implementation*

Among all the current conveyers, the current conveyer II is versatile.[34] The V-I characteristics are given as follows: $V_x = V_y, i_y = 0$, and $i_z = \pm i_x$. $i_z = i_x$ is referred to positive-type current conveyer(CCII+), while $i_z = -i_x$ is referred to negative-type current conveyer (CCII−). CCIIs are implemented by AD844, and it consists of a CCII+ and a voltage buffer.

Based on the dimensionless state equations and the improved module-based method, the attractor of Eq. (4) is implemented by analog circuit. The multiwing-multiscroll compound chaotic attractor circuit based on CCII is shown in Fig. 11(a), where U1, U2 and U3 are integrators, and A1, A2, A3, A4, A5 and A6 are multipliers realized by AD633, and D is the inverting amplifier. The circuits of switching controller S1, S2 are shown as Fig. 11(b). The circuits of nonlinear function $G(x), F(x)$ are presented in Figs. 12(a) and 12(b), respectively.

According to Eq. (4) and the given parameters, the function $f_1(x), f_2(x), f_1(y), f_2(y), f_1(z), f_2(z)$ in Fig. 11(a) are obtained as

$$\begin{cases} f_1(x) = -(z - l), \\ f_2(x) = 100y - 10x, \\ f_1(y) = -(-x - (z - l) - \beta y + G(x)), \\ f_2(y) = 0.1(24 - 4c)x - 0.1(1/p)xz + cy, \\ f_1(z) = -y, \\ f_2(z) = F(0.1x) - 8/3z. \end{cases} \tag{15}$$

Considering the parasitic of AD844, we choose its circuit elements $R_x = 50\Omega$, $R_y = 10\,\mathrm{M}\Omega$, $R_z = 3\,\mathrm{M}\Omega$, $C_y = 2\,\mathrm{pF}$, $C_z = 4.5\,\mathrm{pF}$. The nonlinear circuit system as

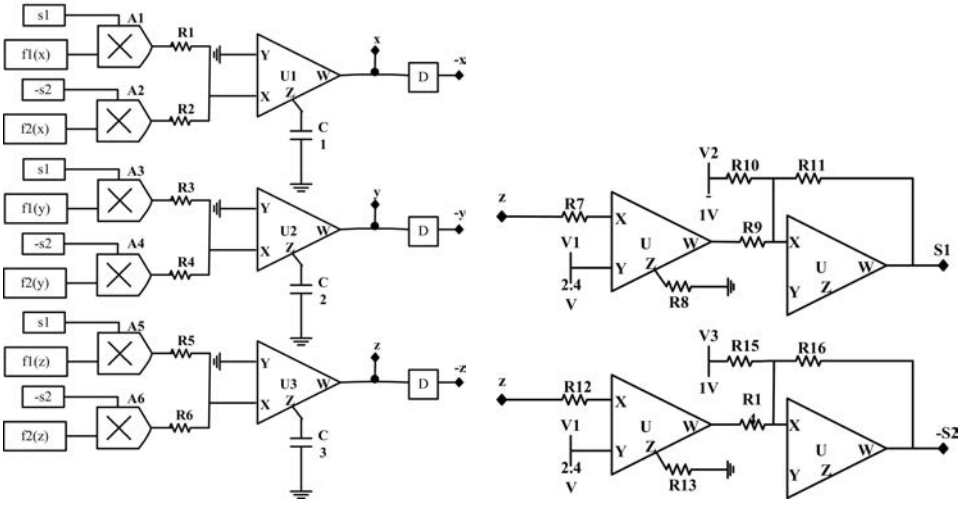

(a) (b)

Fig. 11. Design of system circuits: (a) Circuit of the compound chaotic attractor, (b) Circuits for switching controllers $S_1, -S_2$.

shown in Fig. 11(a) is described by

$$\begin{cases} \dot{x} = S_1 f_1(x)/((R_1 + R_x)(C_1 + C_z)) + S_2 f_2(x)/((R_2 + R_x)(C_1 + C_z)), \\ \dot{y} = S_1 f_1(y)/((R_3 + R_x)(C_3 + C_z)) + S_2 f_2(y)/((R_4 + R_x)(C_2 + C_z)), \\ \dot{z} = S_1 f_1(z)/((R_5 + R_x)(C_3 + C_z)) + S_2 f_2(z)/((R_6 + R_x)(C_3 + C_z)). \end{cases} \tag{16}$$

Let $C_1 = C_2 = C_3 = 100\,\text{nF}$, and compare Eq. (16) with Eq. (4), the resistance values in Figs. 11 and 12 are obtained by $R_1 = R_2 = R_3 = R_4 = R_5 = R_6 = 10\,\text{k}\Omega$,

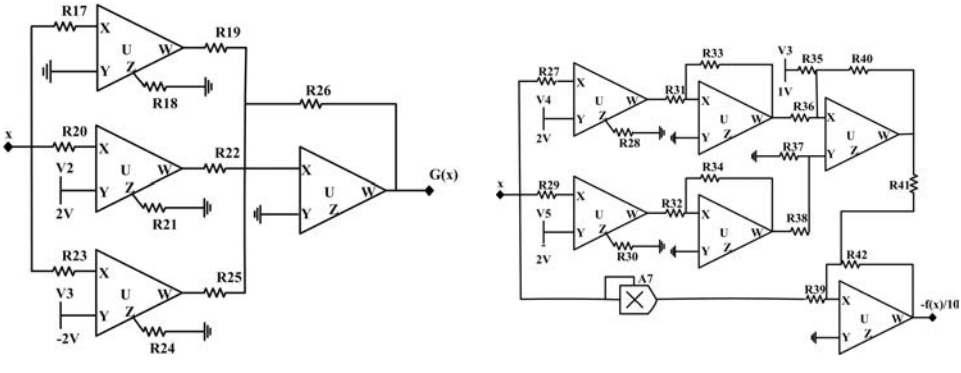

(a) (b)

Fig. 12. Circuits for nonlinear functions $G(x)$ and $F(x)$: (a) For $G(x)$, (b) For $F(x)$.

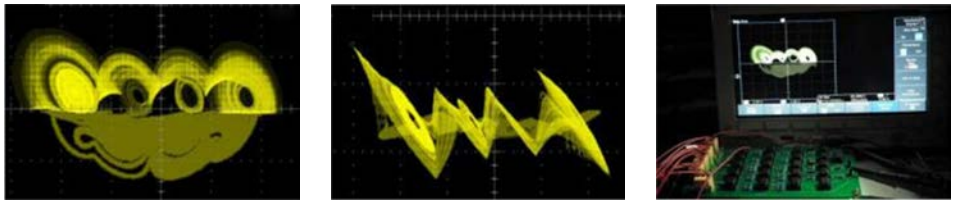

(a) (b) (c)

Fig. 13. Circuit experimental results of the compound multiwing-multiscroll chaotic attractors: (a) Phase diagram on x–z, (b) Phase diagram on x–y, (c) Hardware circuit experiment.

$R_7 = R_{12} = R_{17} = R_{20} = R_{23} = R_{27} = R_{29} = 470\,\Omega$, $R_8 = R_{13} = R_{18} = R_{21} = R_{24} = R_{28} = R_{30} = 5\,\mathrm{M}\Omega$, $R_9 = R_{14} = R_{19} = R_{22} = R_{25} = R_{31} = R_{32} = 11.4\,\mathrm{k}\Omega$, $R_{11} = R_{16} = 500\,\Omega$, $R_{10} = R_{15} = R_{33} = R_{34} = 1\,\mathrm{k}\Omega$, $R_{35} = R_{40} = R_{38} = 10\,\mathrm{k}\Omega$, $R_{37} = 5\,\mathrm{k}\Omega$, $R_{39} = 50\,\mathrm{k}\Omega$, $R_{41} = 96.5\,\mathrm{k}\Omega$, $R_{42} = 200\,\mathrm{k}\Omega$.

The hardware circuit is implemented by using electronic components. All the supply voltages are set to $\pm 15\,\mathrm{V}$. The circuit experimental results are obtained as shown in Fig. 13, it is consistent with Fig. 2(a). Because the center frequency of multiwing chaotic system is totally different with that of multiscroll chaotic system, so we use digital oscilloscope to observe the complete phase diagram.

4.2. *DSP implementation*

The digital circuit of Jerk–Jerk–Lorenz–Lorenz system is implemented based on DSP technique. There are four parts to realize it as shown in Fig. 14. The CPU is DSP TMS320F2812, and the DA converter DAC8552 is a 16-bit dual-channel converter. It is controlled by the DSP board via SPI interface, and the converted data is sent to the oscilloscope, which is used to record phase portraits of the system.[26]

We set the same values of the system parameters in DSP experiment, including step size $h = 0.01$, initial value $(x, y, z) = (0.1, 0.1, 0.1)$, and the phase diagram is shown in Fig. 15. It is consistent with the computer simulation result as shown in Fig. 4(a). It is worth mentioning that the differential equations are solved by employing modified Euler method in DSP implementation.[35] The precision is lower than that of the computer simulation which employs the fourth-order Runge Kutta

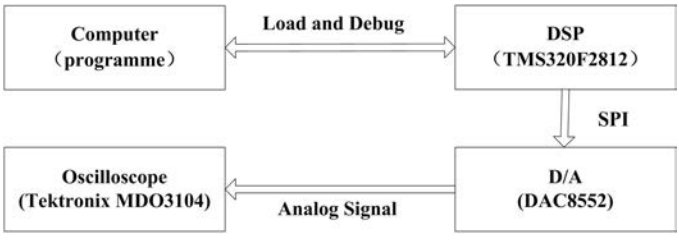

Fig. 14. Structure diagram of DSP implementation.

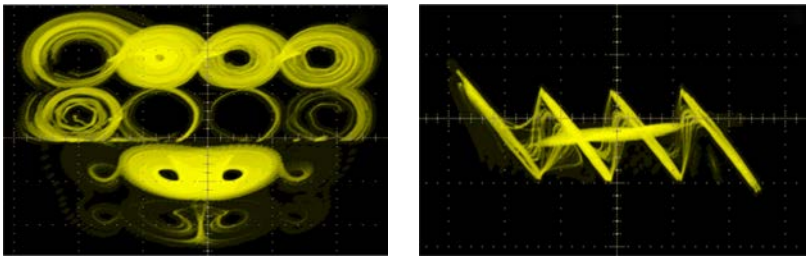

(a) (b)

Fig. 15. DSP Experimental results of the Jerk–Jerk–Lorenz–Lorenz chaotic system: (a) Phase diagram on x–z, (b) Phase diagram on x–y.

method, so the distribution uniformity of attractor shown in oscilloscope is a little different from the computer simulation results.

5. Conclusions

In this paper, four types of grid compound chaotic attractors are designed via switching control. The characteristics of the compound chaotic systems have been investigated by Poincaré section, LLE, and bifurcation diagram. The results show that the LLE of Jerk–Lorenz–Jerk–Lorenz and Jerk–Jerk–Lorenz–Lorenz systems are several times larger than that of other chaotic systems, and the LLE of the Jerk–MirrorLorenz–Jerk system is as large as that of the 1×4-wing Lorenz system. By choosing suitable combination, the LLE of the compound system increases. It is in favor of improving the security of chaotic secure communication system. The pseudorandom switching method has a great potential for applications. Circuit and DSP experiments show a good agreement with numerical simulation results. We found that the grid compound attractor has complex dynamics, and its application in secure communication is our next work.

Acknowledgments

This work is supported by the National Natural Science Foundation of China (Grant Nos. 61161006, 61573383), and the Innovation Project of Graduate of Central South University (Grant No. 2018zzts350).

References

1. E. Lorenz, *J. Atmos. Sci.* **20**, 130 (1963).
2. S. He, K. Sun, X. Mei, B. Yan and S. Xu, *Eur. Phys. J. Plus.* **132**, 36 (2017).
3. M. Fen, *Chaos Soliton Fract* **95**, 200 (2017).
4. X. Han, Y. Yu and C. Zhang, *Nonlinear Dyn.* **88**, 2889 (2017).
5. X. Zhang and Y. Qi, *IET Circuits Devices Syst.* **11**, 437 (2017).
6. Z. Hua, S. Yi, Y. Zhou, C. Li and Y. Wu, *IEEE T. Cybernetics.* **48**, 463 (2018).

7. L. Zhang, K. Sun, S. He, H. Wang and Y. Xu, *Eur. Phys. J. Plus* **132**, 31 (2017).
8. X. Zhang and S. Yu, *Chin. Phys. B* **25**, 83 (2016).
9. L. Zhou, C. Wang and L. Zhou, *Nonlinear Dyn.* **85**, 1 (2016).
10. F. Yuan, G. Wang and X. Wang, *Chaos* **26**, 073107 (2016).
11. K. Bouallegue, *Chaos* **25**, 073108 (2015).
12. S. Yu, J. Lü, X. Yu and G. Chen, *IEEE Trans. Circuits Syst.* **59**, 1015 (2012).
13. N. Slimane, K. Bouallegue and M. Machhout, *Nonlinear Dyn.* **88**, 1655 (2017).
14. Y. Guo, G. Qi and Y. Hamam, *Nonlinear Dyn.* **85**, 1 (2016).
15. K. Bouallegue and C. Toumi, *Chaos Soliton Fract* **44**, 79 (2011).
16. R. Escalante-González and E. Campos-Cantón, *Int. J. Mod. Phys. C* **28**, 1750008 (2016).
17. C. Zhang and S. Yu, *Int. J. Circuits Theor. App.* **41**, 221 (2013).
18. C. Wang, X. Liu and H. Xia, *Chaos* **27**, 033114 (2017).
19. C. Liu, J. Yi, X. Xi, L. An, Y. Qian and Y. Fu, *Procedia Eng.* **29**, 957 (2012).
20. L. Chen, W. Pan and R. Wu, *Chaos* **26**, 084303 (2016).
21. Z. Chen, G. Wen, H. Zhou and J. Chen, *Optik* **130**, 594 (2016).
22. C. Zhang, S. Yu and G. Chen, *Int. J. Bifurcation Chaos* **22**, 1250120 (2012).
23. X. Ai, K. Sun and S. He, *Acta Phys. Sin.* **63**, 040503 (2014).
24. T. Matsumoto, S. Tanaka and L. Chua, *Phys. Rev. A* **30**, 1155 (1984).
25. Y. Ma, Y. Li and X. Jiang, *Chaos Soliton Fract* **75**, 127 (2015).
26. H. Wang, K. Sun and S. He, *Phys. Scr.* **90**, 015206 (2015).
27. Y. Lin and C. Wang, *Electron. Lett.* **52**, 1295 (2016).
28. C. Wang, X. Luo and Z. Wan, *Optik* **125**, 6716 (2014).
29. T. Zuo, K. Sun, X. Ai and H. Wang, *IEEE Trans. Circuits Syst.* **61**, 818 (2014).
30. X. Ai, K. Sun, S. He and H. Wang, *Int. J. Bifurcation Chaos* **25**, 1530027 (2015).
31. K. Sun and J. Sprott, *Int. J. Bifurcation Chaos* **19**, 1357 (2009).
32. S. Yu, J. Lü, H. Leung and G. Chen, *IEEE Trans. Circuits Syst.* **52**, 1459 (2005).
33. H. Liu, *Nonlinear Dyn.* **85**, 1 (2015).
34. A. Lahiri, *Act. Passive Electron. Compon.* **2011**, 274394 (2011).
35. G. Hahn, *Int. J. Numer. Methods Eng.* **32**, 943 (1991).